Eur. Phys. J. Spec. Top. (2023) 232:1171–1175
https://doi.org/10.1140/epjs/s11734-023-00856-y

THE EUROPEAN PHYSICAL JOURNAL SPECIAL TOPICS

Regular Article

Towards the theory of how a constitutional supercooling layer appears ahead of the planar crystallization front

Dmitri V. Alexandrov[1] and Liubov V. Toropova[2,3,a]

[1] Laboratory of Multi-Scale Mathematical Modeling, Laboratory of Stochastic Transport of Nanoparticles in Living Systems, Department of Theoretical and Mathematical Physics, Ural Federal University, Lenin ave., 51, Ekaterinburg 620000, Russian Federation
[2] Laboratory of Mathematical Modeling of Physical and Chemical Processes in Multiphase Media, Ural Federal University, Lenin ave., 51, Ekaterinburg 620000, Russian Federation
[3] Otto-Schott-Institut für Materialforschung, Friedrich-Schiller-Universität-Jena, Jena 07743, Germany

Received 13 February 2023 / Accepted 26 April 2023 / Published online 10 May 2023

Abstract This study, the effect of constitutional supercooling appearing ahead of the crystallization front and leading to the mushy layer origination is considered. An approximate analytical theory determining the time of mushy layer initiation is constructed. Theoretical predictions are in good agreement with numerical simulations carried out in previous studies.

1 Introduction

Phenomena of directional crystallization of supercooled and supersaturated liquids are the basis of many technological processes of metal production and are broadly encountered in nature during freezing of water and solidification of lava [1–10]. The driving force of such processes is the temperature or concentration gradient that defines the spatial crystallization direction of the system. In this case, the phase transformation can take place with a sharp frontal boundary separating purely solid and liquid phases. In addition to this situation, a phase transformation may take place in an extended domain (two-phase layer) that consists of complex entwined structures of solids between which there is a liquid phase [11–16]. In this area, both directional growth of the solid phase and bulk phase transformation (nucleation and growth of nuclei [17–20], evolution of dendritic crystals [21–25]) may occur. A good example of a two-phase layer in nature is the ice slush, which cannot freeze completely. The ice displaces seawater around it, the salinity of which becomes so great that it remains in a liquid state inside the pack ice during the winter season.

This paper deals with the formation of a two-phase (mushy) layer of constitutional supercooling in the process of directional crystallization. Due to the impurity displacement by the growing solid phase (crystallization front), the impurity concentration ahead of the front in liquid accumulates and, at some point in time, the concentration gradient $-m\partial C/\partial z$ (m is the equilibrium liquidus slope) begins to exceed the temperature gradient $\partial T_\ell/\partial z$ at the front (C and T_ℓ are the impurity concentration and temperature in liquid, z is the spatial coordinate of crystallization process). At later moments, a layer of constitutional supercooling arises ahead of the front, and the transition of the crystallizing system from a planar front to a two-phase (mushy) layer model is determined by the equality of aforementioned gradients [26–28]. Below a theory of transition of directional crystallization from a planar front model to a mushy layer model is constructed, in which the processes of solid phase growth can be more complex.

2 The model and its solution

Let us consider the crystallization process in the region of length L. In the melt ($Z(t) < z < L$) and solid ($0 < z < Z(t)$) phases, the thermal conductivity and impurity diffusion equations hold true

$$\frac{\partial T_\ell}{\partial t} = a_\ell \frac{\partial^2 T_\ell}{\partial z^2}, \quad Z(t) < z < L, \tag{1}$$

Structural Transformations and Non- Equilibrium Phenomena in Multicomponent Disordered Systems. Guest editors: Liubov Toropova, Irina Nizovtseva.

[a] e-mails: liubov.toropova@uni-jena.de; l.v.toropova@urfu.ru (corresponding author)

$$\frac{\partial T_s}{\partial t} = a_s \frac{\partial^2 T_s}{\partial z^2}, \quad 0 < z < Z(t), \tag{2}$$

$$\frac{\partial C}{\partial t} = D \frac{\partial^2 C}{\partial z^2}, \quad Z(t) < z < L, \tag{3}$$

where T_s is the solid phase temperatures, a_ℓ and a_s are the thermal diffusivity coefficients of liquid and solid phases, D is the impurity diffusion coefficient (impurity diffusion in the solid phase is traditionally neglected), Z represents the coordinate at time t.

At the phase transition boundary, the temperature continuity condition, the equality of temperature to the phase transition temperature, and the heat and mass balances are fulfilled. Namely,

$$T_\ell = T_s, \quad z = Z(t), \tag{4}$$

$$T_\ell = T_* - mC, \quad z = Z(t), \tag{5}$$

$$\lambda_s \frac{\partial T_s}{\partial z} - \lambda_\ell \frac{\partial T_\ell}{\partial z} = L_V \frac{dZ(t)}{dt}, \quad z = Z(t), \tag{6}$$

$$(1-k)C\frac{dZ(t)}{dt} + D\frac{\partial C}{\partial z} = 0, \quad z = Z(t). \tag{7}$$

Here, T_* represents the phase transition temperature of pure melt, λ_s and λ_ℓ are the thermal conductivity coefficients of solid and melted phases, respectively, L_V is latent heat of solidification, k is the impurity segregation coefficient, which is equal to the ratio of impurity concentration C_s in the solid phase to the impurity concentration in melt at the crystallization front, i.e.

$$k = \frac{C_s}{C}, \quad z = Z(t). \tag{8}$$

As the diffusion of impurity in the solid phase is neglected, relation (8) gives the value of the impurity concentration absorbed by the flat solidification front at each time moment and, thus, allows us to determine the concentration profile in the solid phase.

At the right boundary, $z = L$, we set the condition of its impermeability for the impurity and fix the heat flux as

$$\frac{\partial C}{\partial z} = 0, \quad z = L, \tag{9}$$

$$\frac{\partial T_\ell}{\partial z} = g_\ell, \quad z = L, \tag{10}$$

where g_ℓ is the given temperature gradient.

At the left boundary, $z = 0$, we set the condition of its smoothly increasing cooling with time in the form of

$$\lambda_s \frac{\partial T_s}{\partial z} = \lambda_\ell g_\ell + \alpha t, \quad z = 0, \tag{11}$$

where α is the cooling coefficient.

As the initial conditions, we set the position of the crystallization front, as well as the temperature and concentration profiles of the following form

$$Z(0) = \varepsilon L, \tag{12}$$

$$T_\ell = T_* - mC_\infty + g_\ell(z - Z(0)), \quad t = 0, \quad Z(0) < z < L, \tag{13}$$

$$T_s = T_* - mC_\infty + \frac{\lambda_\ell}{\lambda_s} g_\ell (z - Z(0)), \quad t = 0, \quad 0 < z < Z(0), \tag{14}$$

$$C = C_\infty, \quad t = 0, \quad Z(0) < z < L, \tag{15}$$

where C_∞ is the constant impurity concentration at the initial moment of time and $\varepsilon \ll 1$ is a small parameter.

Thus, initially, the crystallization front is supposed to already exist at some small distance from the left boundary. The linear temperature profile is given with its slope on both sides of the crystallization front. At the initial moment $t = 0$, the difference of heat at the front is zero and, hence, the velocity dZ/dt of the front, according to the boundary condition (6), is also zero.

The time t_* of the two-phase layer origination is defined from the condition of constitutional supercooling [26–28]

$$-m\frac{\partial C}{\partial z} = \frac{\partial T_\ell}{\partial z}, \quad z = Z(t). \tag{16}$$

The model (1)–(16) was numerically analyzed in Refs. [27, 29], and condition (16) corresponding to the narrow quasi-equilibrium two-phase layer approximation was used in the case of constitutional supercooling [27]. Note that the relation $-m\frac{\partial C}{\partial z} > \frac{\partial T_\ell}{\partial z}$ is satisfied when there is a supercooled liquid region ahead of the solidification front.

Figure 1 represents the results of these calculations for an iron-nickel alloy at time $t = 360$ s (a) and $t_* = 221.9$ s (b), respectively. The calculations showed that the temperature profiles in both phases during the entire crystallization time remain almost linear functions of the spatial coordinate, which is also clearly visible from Fig. 1. This result can be explained by the fact that the relaxation times of the temperature fields in both phases are several orders of magnitude shorter than the relaxation time of the diffusion field. It is also obvious from the calculations that in the case when the length of the two-phase layer between the solid phase and the melt is sufficiently small, its presence has certain differences in the character of the impurity distribution over the solid phase in comparison with the standard formulation of the problem on solidification with a flat solidification front. In this case, the concentration of impurity in the solid phase will monotonically grow with the increasing spatial coordinate, as shown in Fig. 1b.

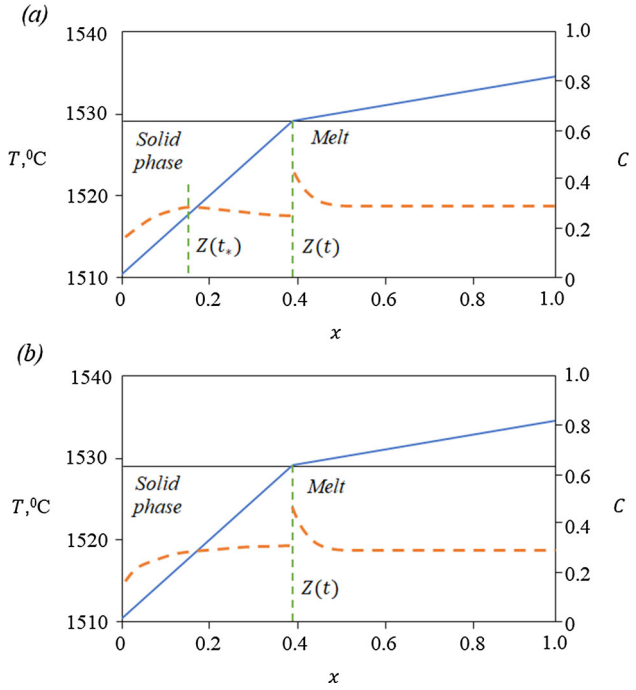

Fig. 1 Concentration (dashed lines) and temperature (solid lines) profiles, phase transition temperature (horizontal straight line) and position $Z(t)$ of the crystallization front during solidification of iron-nickel melt at: **a** $t = 360$ s; **b** $t = 221.9$ s. Point $t = t_*$ corresponds to the maximum impurity concentration in the solid phase, $x = z/L$. Calculation parameters are: $m = 2.65$ °C, $k = 0.68$, T_*=1529.5 °C, $L_V = 3398.5$ cal/cm^3, $D = 5 \cdot 10^{-5}$ cm^2/s, $C_\infty = 0.3$, $\lambda_s = 0.177$ cal/(s cm °C), $\lambda_\ell = 0.1$ cal/(s cm °C), $\alpha = 0.02$ cal/(s^2 cm^2), $a_s = 0.25$ cm^2 /s, $a_\ell = 0.14$ cm^2 /s, g_ℓ 10 °C/cm, $\varepsilon = 0.01$, $L = 1$ cm

The linearity of the temperature profiles at all times, clearly visible in Fig. 1a and b, allows us to approximate Equs. (1) and (2) by their stationary analogs

$$\frac{\partial^2 T_\ell}{\partial z^2} = 0,\ Z(t) < z < L; \quad \frac{\partial^2 T_s}{\partial z^2} = 0,\ 0 < z < Z(t), \tag{17}$$

whose solution has the form

$$T_\ell(t,z) = A_1(t) + A_2(t)z, \quad T_s(t,z) = B_1(t) + B_2(t)z. \tag{18}$$

Substitution of solutions (18) into conditions (10), (11), and (4) defines the coefficients A_2, B_2 and the linear combination between the coefficients A_1 and B_1 as

$$A_1(t) = B_1(t) + \left(\frac{\lambda_\ell}{\lambda_s} g_\ell - g_\ell + \frac{\alpha}{\lambda_s} t\right) Z(t), \tag{19}$$

$$A_2 = g_\ell, \quad B_2(t) = \frac{\lambda_\ell}{\lambda_s} g_\ell + \frac{\alpha}{\lambda_s} t. \tag{20}$$

Then, substituting the distributions (18) into the boundary condition (6), and considering (19), we obtain

$$\frac{dZ}{dt} = \frac{\alpha}{L_V} t = \mu t. \tag{21}$$

This condition representing a linear law for the crystallization rate, agrees perfectly with numerical calculations carried out in Ref. [27].

Let us now find the time t_* of the two-phase layer origination. Considering a reference frame moving with the velocity μt and introducing the new variable $q(t,y) = C(t,y) - C_\infty$, we obtain the following problem

$$\frac{\partial q}{\partial t} = \mu t \frac{\partial q}{\partial y} + D\frac{\partial^2 q}{\partial y^2}, \quad 0 < y < \infty, \tag{22}$$

$$(1-k)\mu t q + (1-k)\mu t C_\infty + D\frac{\partial q}{\partial y} = 0, \quad y = 0, \tag{23}$$

$$\frac{\partial q}{\partial y} = 0, \quad y \to \infty, \tag{24}$$

$$q = 0, \quad t = 0. \tag{25}$$

At time t_*, the impurity concentration in liquid takes a maximum value in the whole occupied volume for any coordinate y. We take the left part of Eq. (22) and integrate the result over y from zero to infinity. Using condition (24) and the relation $q \to 0$ at $y \to \infty$, we get

$$q = \frac{D g_\ell}{m \mu t_*}, \quad y = 0, \quad t = t_*. \tag{26}$$

Here we also assumed that according to (16), (18) and (20) $\partial q/\partial y = -g_\ell/m$ at $y = 0$, $t = t_*$. Combining relations (23) and (26), we find the time of two-phase layer origination and the impurity concentration at the front as

$$t_* = \frac{kDg_\ell}{(1-k)\mu m C_\infty}, \quad C = \frac{C_\infty}{k}, \quad y = 0, \quad t = t_*. \tag{27}$$

Figure 2 shows the dependence of the two-phase laayer origination on the cooling parameter α (note that $\mu = \alpha/L_V$). As can be easily seen, expression (27) agrees well with the numerical solution of the problem obtained in Ref. [29].

Let us now consider the concentration problem (22)–(25) at sufficiently small times after the beginning of the crystallization process and represent the concentration q as an expansion $q = q_0 + q_1 + q_2 + \ldots$, when each subsequent summand is assumed to be much smaller than the previous one. Then we find q_0 and q_1 as

$$\frac{\partial q_0}{\partial t} = D\frac{\partial^2 q_0}{\partial y^2}, \ 0 < y < \infty;$$

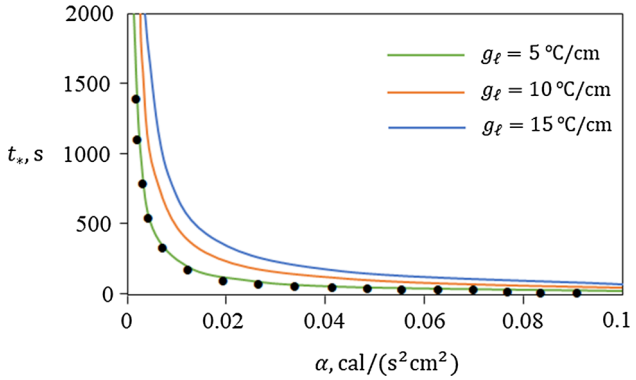

Fig. 2 The time t_* for the two-phase layer origination versus the cooling parameter α for different gradients g_ℓ. The points are the results of numerical solution according to Ref. [29]

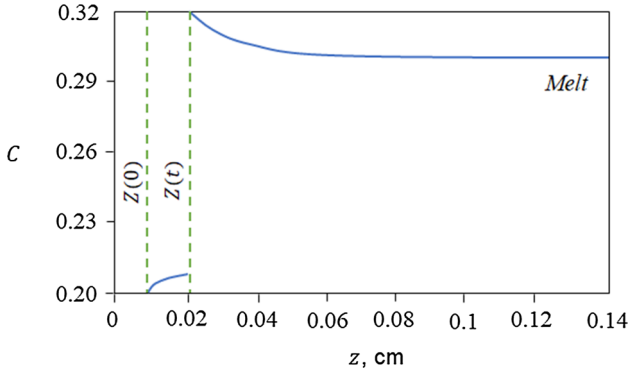

Fig. 3 The distribution of impurities in the solid and liquid phases at time $t = 10$ s (solid lines) and the positions of the crystallization front (dashed lines). The concentrations of impurities in the liquid and solid phases at the front are 0.319 and 0.217, respectively, and the position of the crystallization front is 0.013 cm. Parameter $\alpha = 0.2$ cal/(s^2 cm^2)

$$(1-k)\mu t C_\infty + D\frac{\partial q_0}{\partial y} = 0, \quad y = 0, \tag{28}$$

$$\frac{\partial q_1}{\partial t} = \mu t \frac{\partial^2 q_0}{\partial y^2} + D\frac{\partial^2 q_1}{\partial y^2}, \quad 0 < y < \infty;$$
$$(1-k)\mu t q_0 + D\frac{\partial q_1}{\partial y} = 0, \quad y = 0 \tag{29}$$

with conditions (24) and (25) taking the form

$$\frac{\partial q_i}{\partial y} = 0, \quad y \to \infty; \quad q_i = 0, \quad t = 0 \tag{30}$$

(they are valid for all q_i $(i = 0, 1, ...)$).

Each of the problems (28)–(30) can be solved using the Laplace integral transform. Then, finally, we obtain

$$q_0(t,y) = \frac{C_\infty(1-k)\mu}{\sqrt{\pi D}} \int_0^t \exp\left[-\frac{y^2}{4Df}\right]\frac{t-f}{\sqrt{f}}df, \tag{31}$$

$$q_1(t,y) = \frac{C_\infty(1-k)\mu^2}{2D\sqrt{\pi}}\left(\frac{5}{2}(1-k) - \frac{9}{8} - \frac{9y}{8\sqrt{D}}\right)$$
$$\times \int_0^t \exp\left[-\frac{y^2}{4Df}\right]\frac{(t-f)^2}{\sqrt{f}}df - \frac{C_\infty(1-k)\mu^2 y^2}{192D^2\sqrt{\pi}}$$
$$\times \int_0^t \exp\left[-\frac{y^2}{4Df}\right]\frac{(t-f)^4}{\sqrt{f}}df. \tag{32}$$

Thus, if the solidification process occurs at large cooling coefficients, corresponding to small times t_* according to Fig. 3, the obtained result completely determines the solution of the frontal problem up to the moment of two-phase layer formation.

3 Conclusion

In summary, we have developed the analytical theory describing the mushy layer initiation ahead of a planar solid— liquid interface due to the effect of constitutional supercooling. This effect leans upon the process of impurity displacement by the growing solid–liquid interface into the liquid (melt) phase. As this takes place, the smaller the segregation coefficient, the more the impurity is displaced and the faster the concentration supercooling sets in. The analytical theory under consideration enables us to find the time t_* of mushy layer incipience corresponding to switching from a mathematical model with a planar front to a model with a two-phase (mushy) layer. In other words, at this point in time, a supercooled region forms ahead of the purely solid phase, where complex dendrite-like structures can grow and new crystallites can nucleate.

Generally speaking, when constitutional supercooling occurs (after a lapse of time t_*), one of the two-phase layer models (e.g. quasi-equilibrium, weakly or highly nonequilibrium) [14–16, 30–37] should be used to describe the crystallization process. In addition, the crystallization process may be influenced by dynamic instability of the two-phase layer (e.g. leading to self-oscillation of this layer) [38–42], convective fluid currents (e.g. forming channels in this layer) [43–45], additional impurity components (e.g. forming cotectic region) [46, 47], etc. These questions represent important research directions in the theory of crystallization with a two-phase layer.

Acknowledgements This study was financially supported by the Russian Science Foundation (Project No. 21-79-10012).

Funding Information Open Access funding enabled and organized by Projekt DEAL.

Data Availability Statement All data generated or analysed during this study are included in this published article.

References

1. W. Kurz, D.J. Fisher, *Fundamentals of solidification* (Trans. Tech. Publ, Aedermannsdorf, 1989)
2. D. Herlach, P. Galenko, D. Holland-Moritz, *Metastable Solids from Undercooled Melts* (Elsevier, Amsterdam, 2007)
3. H.E. Huppert, J. Fluid Mech. **212**, 209 (1990)
4. D.V. Alexandrov, A.P. Malygin, I.V. Alexandrova, Ann. Glaciol. **44**, 118 (2006)
5. D.V. Alexandrov, I.G. Nizovtseva, Int. J. Heat Mass Trans. **51**, 5204 (2008)
6. D.V. Alexandrov, A.P. Malygin, Phys. Earth Planet. Inter. **189**, 134 (2011)
7. D.V. Alexandrov, A.V. Netreba, A.P. Malygin, Int. J. Heat Mass Trans. **55**, 1189 (2012)
8. D. Notz, M.G. McPhee, M.G. Worster, G.A. Maykut, K.H. Schlünzen, H. Eicken, J. Geophys. Res. **108**, 3223 (2003)
9. M.G. McPhee, G.A. Maykut, J.H. Morison, J. Geophys. Res. **92**, 7017 (1987)
10. D.V. Alexandrov, A.Y. Zubarev, Philos. Trans. R. Soc. A **377**, 20180353 (2019)
11. D.V. Alexandrov, D.L. Aseev, Comput. Mater. Sci. **37**, 1 (2006)
12. D.V. Alexandrov, A.A. Ivanov, J. Exper. Theor. Phys. **108**, 821 (2009)
13. I.G. Nizovtseva, D.V. Alexandrov, Philos. Trans. R. Soc. A **378**, 20190248 (2020)
14. R.N. Hills, D.E. Loper, P.H. Roberts, Q. J. Appl. Maths. **36**, 505 (1983)
15. A.C. Fowler, IMA, J. Appl. Math. **35**, 159 (1985)
16. V.T. Borisov, *Theory of Two-Phase Zone of a Metal Ingot* (Metallurgiya Publishing House, Moscow, 1987)
17. D.V. Alexandrov, J. Phys. A: Math. Theor. **51**, 075102 (2018)
18. D.V. Alexandrov, I.G. Nizovtseva, I.V. Alexandrova, Int. J. Heat Mass Trans. **128**, 46 (2019)
19. D.V. Alexandrov, I.V. Alexandrova, Philos. Trans. R. Soc. A **378**, 20190247 (2020)
20. D.V. Alexandrov, A.A. Ivanov, I.G. Nizovtseva, S. Lippmann, I.V. Alexandrova, E.V. Makoveeva, Crystals **12**, 949 (2022)
21. P.K. Galenko, V.A. Zhuravlev, *Physics of Dendrites* (World Scientific, Singapore, 1994)
22. D.V. Alexandrov, P.K. Galenko, J. Phys. Chem. Solids **108**, 98 (2017)
23. J. Gao, A. Kao, V. Bojarevics, K. Pericleous, P.K. Galenko, D.V. Alexandrov, J. Cryst. Growth **471**, 66 (2017)
24. D.V. Alexandrov, P.K. Galenko, Philos. Trans. R. Soc. A **379**, 20200325 (2021)
25. P.K. Galenko, L.V. Toropova, D.V. Alexandrov, G. Phanikumar, H. Assadi, M. Reinartz, P. Paul, Y. Fang, S. Lippmann, Acta Mat. **241**, 118384 (2022)
26. M.G. Worster, J. Fluid Mech. **167**, 481 (1986)
27. Y.A. Buyevich, D.V. Alexandrov, V.V. Mansurov, *Macrokinetics of Crystallization* (Begell House, New York, 2001)
28. I.V. Alexandrova, D.V. Alexandrov, D.L. Aseev, S.V. Bulitcheva, Acta Phys. Pol. A **115**, 791 (2009)
29. D.V. Alexandrov, M. E. Komarovskii, in *Proceedings of 19th Russian Conference on Structure and Properties of Metallic and Slag Melts*, (Yuzhno-Ural. Gos. Univ., Chelyabinsk, 2001), Vol. 4, pp. 98–103
30. Y.A. Buyevich, L.Y. Iskakova, V.V. Mansurov, Can. J. Phys. **68**, 790 (1990)
31. L.V. Toropova, A.A. Ivanov, S.I. Osipov, Y. Yang, E.V. Makoveeva, D.V. Alexandrov, J. Phys.: Condens. Matter **34**, 383002 (2022)
32. V.V. Mansurov, Math. Comput. Modell. **14**, 819 (1990)
33. D.V. Alexandrov, Acta Mater. **49**, 759 (2001)
34. L.V. Toropova, D.V. Alexandrov, Sci. Rep. **12**, 10997 (2022)
35. D.V. Alexandrov, L.V. Toropova, Sci. Rep. **12**, 17857 (2022)
36. D.V. Alexandrov, G.Y. Dubovoi, A.P. Malygin, I.G. Nizovtseva, L.V. Toropova, Russ. Metall. (Met.) **2017**(2), 127 (2017)
37. L.V. Toropova, D. Aseev, S. Osipov, A. Ivanov, Math. Methods Appl. Sci. **45**, 8011 (2022)
38. Y.A. Buyevich, V.V. Mansurov, I.A. Natalukha, Chem. Eng. Sci. **46**, 2573 (1991)
39. Y.A. Buyevich, I.A. Natalukha, Chem. Eng. Sci. **49**, 3241 (1994)
40. D.M. Anderson, M.G. Worster, J. Fluid Mech. **302**, 307 (1995)
41. D.V. Alexandrov, A.O. Ivanov, J. Cryst. Growth **210**, 797 (2000)
42. A.A. Ivanov, I.V. Alexandrova, D.V. Alexandrov, Eur. Phys. J. Spec. Top. **229**, 365 (2020)
43. M.G. Worster, R.C. Kerr, J. Fluid Mech. **269**, 23 (1994)
44. T.P. Shulze, M.G. Worster, J. Fluid Mech. **388**, 197 (1999)
45. R.F. Katz, M.G. Worster, J. Comput. Phys. **227**, 9823 (2008)
46. D.M. Anderson, J. Fluid Mech. **483**, 165 (2003)
47. D.V. Alexandrov, A.A. Ivanov, Int. J. Heat Mass Trans. **52**, 4807 (2009)